Available online at www.sciencedirect.com

ScienceDirect

Ceramics International 40 (2014) 6021–6029

CERAMICS INTERNATIONAL

www.elsevier.com/locate/ceramint

Magnesium incorporated hydroxyapatite: Synthesis and structural properties characterization

Arghavan Farzadi[a], Farhad Bakhshi[b], Mehran Solati-Hashjin[a,b,*], Mitra Asadi-Eydivand[a], Noor Azuan abu Osman[a]

[a]Department of Biomedical Engineering, Faculty of Engineering, University of Malaya, 50603 Kuala Lumpur, Malaysia
[b]Biomaterials Center of Excellence, Amirkabir University of Technology, 15914 Tehran, Iran

Received 1 August 2013; received in revised form 6 November 2013; accepted 9 November 2013
Available online 26 November 2013

Abstract

Synthetic hydroxyapatites are widely used in bone tissue engineering because of their similar composition with the inorganic phase of hard tissues. Biological apatites, however, are calcium-deficient apatites with many di- and tri-valent ion substitutions. In this study, stoichiometric hydroxyapatite (HA) powders were prepared by wet-chemical precipitation method, and the effect of Mg incorporation on the resulting solid solution was investigated. X-ray diffraction (XRD) analysis confirmed that the substitution of Mg for Ca in apatite lattice resulted in a slight increase in *a* lattice and more emphasized decrease in *c* lattice parameters: 0.0966% and 0.2964%, respectively. The results indicated an increase in the *d*-spacing of Mg-doped HA (MHA). Scanning electron microscopy–energy dispersive X-ray spectroscopy (SEM–EDX) analysis showed that the Mg, C, and O elements were evenly distributed. Transmission electron microscopy (TEM) analysis revealed that incorporation of Mg did not significantly alter the size of the precipitated crystals. Although XRD patterns suggested smaller crystallite size, such a result was still consistent with TEM results, wherein change in size was not significant in Mg-doped HA (MHA) in comparison to HA. Moreover, the incorporation of impurity ions into the HA lattice did not alter the high-temperature phase stability often required for processing. The comparison of HA and MHA samples before and after heat treatment showed that the apatite structure did not decompose or undergo any phase transformation at high temperatures. A proportion of the Mg added did not substitute into the HA lattice. The $Mg(OH)_2$ phase, as observed in the XRD pattern of the Mg-added sample, was a second phase that was easily washed by a citrate solution. In both HA and MHA samples, the calcium phosphate phase remained as a single-phase hexagonal calcium hydroxyapatite before and after heat treatment.

Keywords: A. Powder; A. Chemical preparation; D. Apatite; E. Biomedical applications; Magnesium substitution

1. Introduction

Among all calcium phosphate bioceramics, hydroxyapatite (HA), $Ca_{10}(PO_4)_6(OH)_2$, is the most extensively used biocompatible ceramic materials for bone tissue engineering, as its chemical composition is similar to the bone mineral phase [1–5]. Biological apatites are nonstoichiometric nanocrystalline carbonated HAs (CHA). Therefore, synthetic HA ceramics are doped with small amounts of additives (e.g., Mg^{2+}, Zn^{2+}, F^-, Mn^{2+}, and CO_3^{2-} ions). Although the substitution does not intensely change the crystallographic properties of HA, it affects the biological and mechanical properties [6–13]. An ionocovalent structural model of the apatite family shows a structure that can accept both cationic and anionic substituents. These substitutions induce modifications in lattice parameters and crystallinity, which substantially influence the solubility of HA at physiological conditions without generating significant changes in the hexagonal system of apatite [14–19].

One of the elements associated with biological apatites is magnesium. Mg incorporation into HA stimulates osteoblast

*Corresponding author at: Department of Biomedical Engineering, Faculty of Engineering, University of Malaya, 50603 Kuala Lumpur, Malaysia. Tel.: +60 37 9674446.
E-mail address: mehran@um.edu.my (M. Solati-Hashjin).

0272-8842
http://dx.doi.org/10.1016/j.ceramint.2013.11.051

proliferation. Mg acts similar to a growth factor during the early stages of osteogenesis and promotes bone formation [19]. Typical concentrations of carbonate and Mg ions in human bone are 5.8 and 0.55 wt%, respectively [7,18]. Although the extent of these elemental substitutions is minimal, they are important for biological activity and interaction between bone mineral and calcium–phosphate-based implant materials by influencing crystal growth, dissolution rate, solubility, surface chemistry and charge, morphology, and the mechanical properties [6,7,9,14,20–22].

By substitution of a smaller Mg ion for a larger Ca ion, additional structural changes may be required to prevent destabilization/decomposition of the structure during heat treatment process. This can be achieved by co-substitution of a second ion, such as CO_3^{2-} to the HA structure [23,18].

The incorporation of Mg ions within the HA structure is essential for developing artificial bone substitutes. This study aims to investigate the synthesis of stoichiometric HA via a wet-chemical precipitation method, and the effect of Mg incorporation on the structure of the resulting Mg–HA solid solution. Various analytical techniques have been employed to study the phase, crystallinity, crystal size, and crystal lattice structure of the Mg-doped HA (MHA) samples.

2. Materials and methods

2.1. Sample preparation

Pure and doped nanocrystalline HA powders were synthesized based on a wet chemical method [6,15,24]. Diammonium hydrogen phosphate [$(NH_4)_2HPO_4$] (Prolabo Merck eurolab no. 21 309.293), calcium nitrate tetrahydrate [$Ca(NO_3)_2 \cdot 4H_2O$] (Prolabo Merck eurolab no. 22 384.298), and magnesium chloride hexahydrate [$MgCl_2 \cdot 6HO$] (Merck no. 105833) were applied as sources of P, Ca, and Mg ions, respectively.

Stoichiometric HA was prepared as a control via a classic precipitation method by dropping 0.29 M aqueous phosphate solution into 0.30 M calcium salt solution for 3 h, while constantly stirring. The starting Ca/P molar ratio was equal to the stoichiometric value of HA (1.67). NaOH (Merck no. 105833) solution was used to control the pH of the solution mixture at 11 during the process. The resulting suspension was aged for 24 h at room temperature, centrifuged, dried in an oven at 70 °C overnight, and calcined at 900 °C in air for 1 h.

Mg-doped HA was prepared by drop-wise addition of an aqueous diammonium hydrogen phosphate solution into a basic solution consisting of magnesium chloride hexahydrate

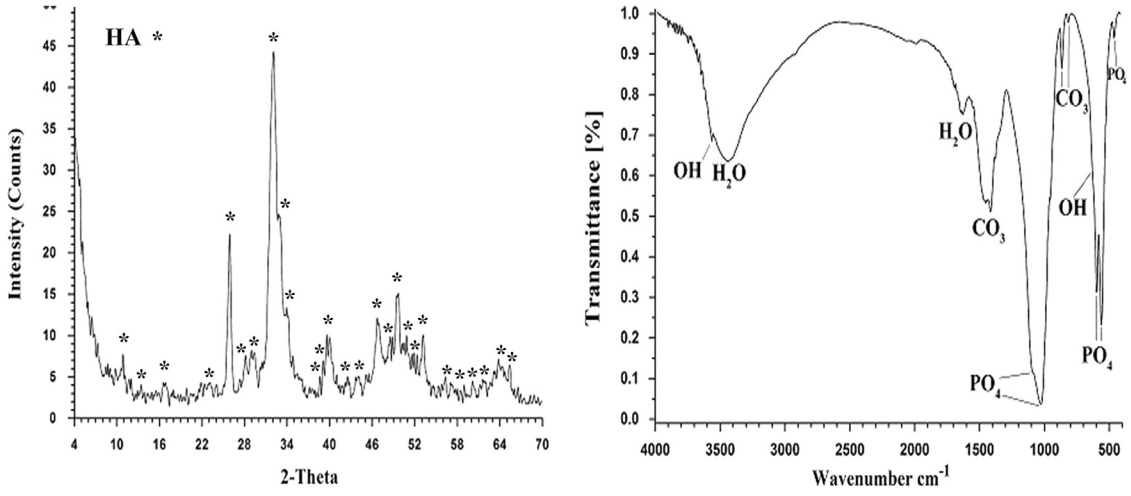

Fig. 1. XRD (a) and FTIR (b) patterns of the as-prepared HA powders.

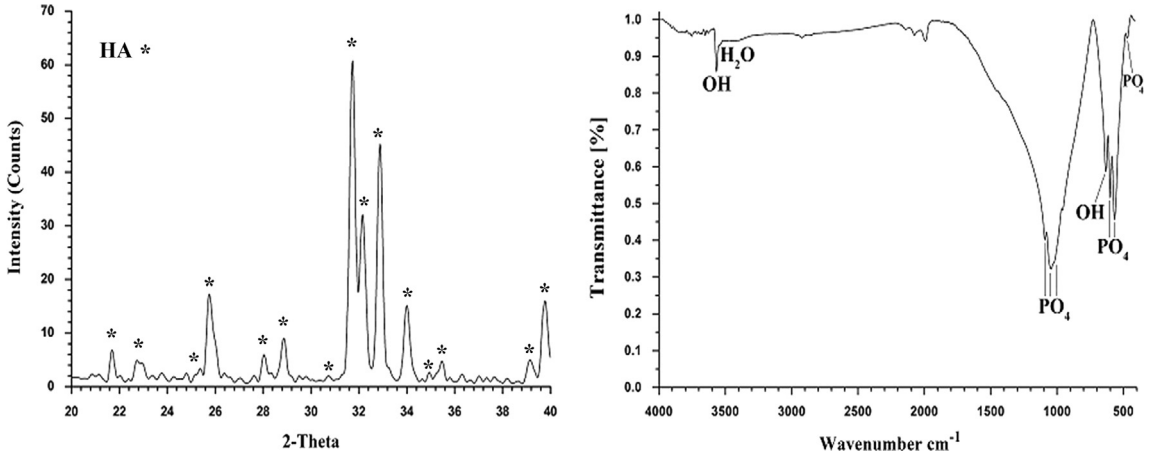

Fig. 2. XRD (a) and FTIR (b) patterns of the calcined HA powders.

and calcium nitrate tetrahydrate with Mg/Ca molar ratio of 0.18 for 3 h. The pH of the suspension was adjusted to 11, and stirred for 24 h. The resulting precipitates were centrifuged and washed three times using distilled water. All samples were dried at 70 °C overnight, calcined at 900 °C for 1 h, and then stored for further analysis.

2.2. Sample characterization

Phase analyses, crystallinity, crystallite size, and lattice parameters of powders were determined by X-ray diffraction (XRD) (Bruker Analytical X-ray Systems, Cu-Kα radiation, 40 kV, 30 mA, and 0.02° s^{-1} step scan). The XRD patterns of the samples (Figs. 1–5) were obtained by using OriginLab OriginPro v9.0 SR2 and PeakFit v.4.12 softwares.

The lattice parameters of HA (before and after calcination) and MHA (before and after calcination) were calculated by Rietveld structure refinement of XRD data from each sample. The degree of crystallinity, corresponding to the crystalline HA, MHA, and calcined phases, were evaluated by Eq. (1), where I_{300} is the intensity of (300) reflection and $V_{112/300}$ is the intensity of the hollow between (112) and (300) reflections, which completely disappears in noncrystalline samples. Broadening of a diffraction peak can be related to crystallite size, which may be smaller or equal to the grain size, through Scherrer's equation shown in Eq. (2), where λ is the wavelength (CuKα), t is the full width at half-maximum of the HA (211) line, and θ is the diffraction angle. The (002), (310), and (222) HA peaks were chosen for the analysis of Bragg line broadening [1,25]:

$$X_C = 1-(V_{112/300}/I_{300}) \quad (1)$$

$$B = \frac{0.9\lambda}{t\ \cos(\theta)} \quad (2)$$

Fourier transform infrared spectroscopy (FTIR) (Equinox 55 Bruker) was performed to evaluate the functional groups and chemical composition of the specimens and quantify the effect of Mg substitution on the different functional groups, such as hydroxyl and phosphate [26]. FTIR pellets of powdered samples were mixed with KBr and the spectra was obtained over the 400–4000 cm^{-1} region. Scanning electron microscopic–energy dispersive X-ray spectroscopy (SEM–EDX) analysis (Tescan Vega 2XMU) was used for morphological observations. Before examination, samples were coated with a thin gold film by sputtering using low deposition rate.

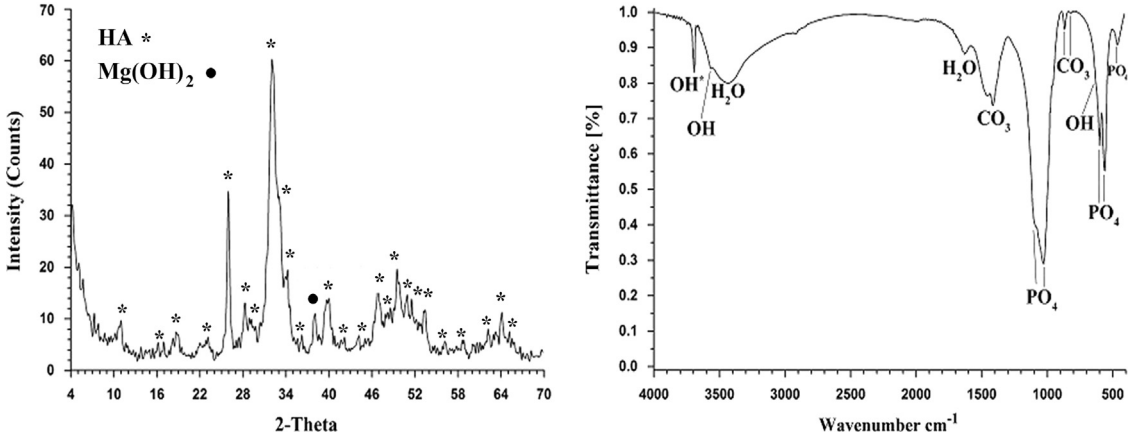

Fig. 3. XRD (a) and FTIR (b) patterns of Mg-substituted HA powders.

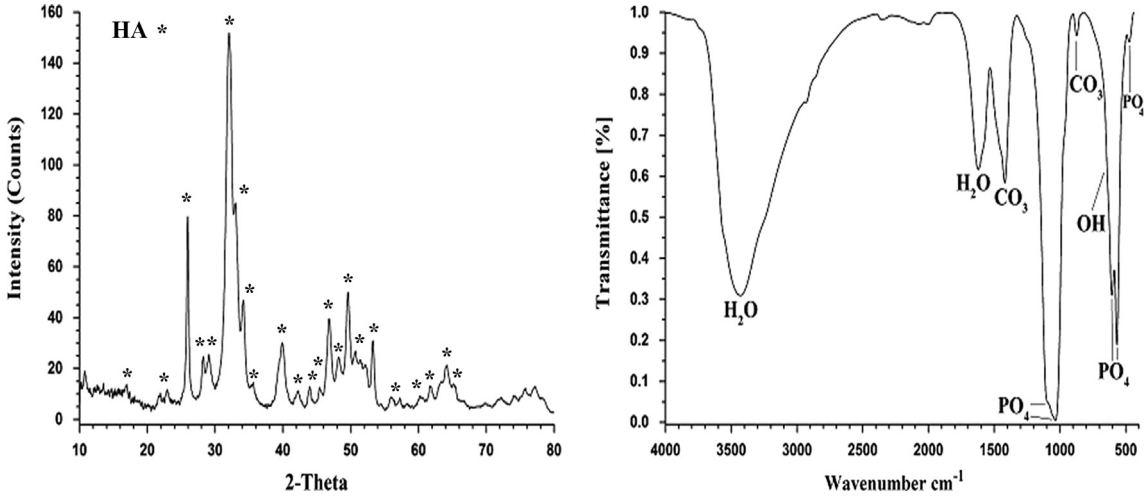

Fig. 4. XRD (a) and FTIR (b) patterns of washed Mg-substituted HA powders (washed MHA).

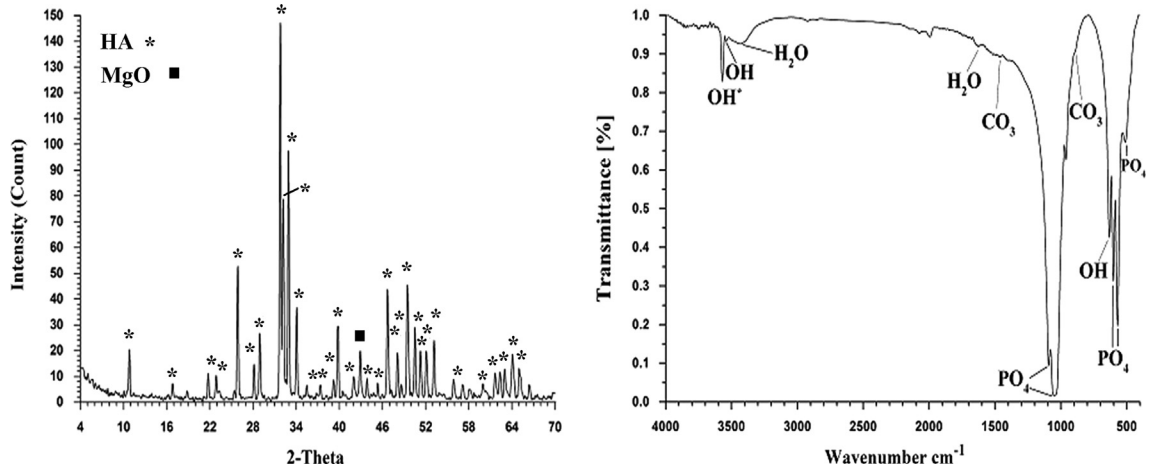

Fig. 5. XRD (a) and FTIR (b) patterns of calcined MHA powders.

In addition, MgHA crystals were observed with a Philips EM 208S transmission electron microscope at 100 keV. Samples for TEM were prepared by spreading a drop of nanoparticles solution in ethanol (~5 mg/mL) onto standard coated copper grid.

3. Result and discussion

The HA peaks were indexed according to the standard pattern (JCPDS 09-0432), as shown in Figs. 1a and 2a. Stoichiometric HA powders exhibited sharp diffraction peaks, indicating high crystallinity of the structure. No impurity phase was identified by XRD.

As shown in Figs. 1(b)–5(b), all FTIR spectra illustrated an OH^- band at 3569 cm^{-1} and PO_4^{3-} bands at 472, 565, 603, and 1032 cm^{-1} associated with HA. The sharp peak (1637 cm^{-1}) and broad bands for adsorbed water (3000–3500 cm^{-1}) are the evidence of water absorption due to the high specific surface area that precipitated powders usually have. The CO_3^{2--} groups, that can substitute both PO_4^{3-} and OH^- ions in the HA structure appeared as 1461, 1423, and 875 cm^{-1} wave numbers. The calcined HA powders exhibited FTIR patterns similar to that of untreated sample, as shown in Fig. 2b. Moreover, the peaks related to absorbed water and carbonates disappeared after heat treatment which means the carbonate is not incorporated in the lattice of HA.

Although Fig. 3a indicates the presence of HA phase in the Mg-substituted sample, the intensity of HA peaks were decreased. This suggests the decrease of crystallinity with reducing grain growth because of Mg ion substitution. Diffractogram of the sample showed additional peaks in the XRD pattern, which were corresponded to $Mg(OH)_2$. As shown in Fig. 3b, the peak marked with "●" at 3698 cm^{-1} was observed in the Mg-doped HA sample. This peak corresponds to the stretching mode of hydroxyl groups that appears when combined with magnesium [27–31], demonstrating the presence of Mg^{+2} in the apatite structure.

The Mg-added sample contained unreacted $Mg(OH)_2$. This was subjected to a washing treatment at room temperature by using 0.2 M (4.2028 g) ammonium citrate aqueous solutions (pH 9) for further characterization and elimination of non-apatitic secondary phase to ensure that measurements are only associated to the effect of magnesium incorporated to the HA lattice and not to the possible impurity $Mg(OH)_2$ second phase [32].

Table 1
Lattice parameters of stoichiometric HA powders according to JCPDS no. 09-0432.

2θ	*d* (A°) (for Sto-HA)	*h*	*k*	*l*	*a* (A°)	*c* (A°)
18.7850	4.7200	1	1	0	9.4400	
21.8190	4.0700	2	0	0	9.3993	
25.8790	3.4400	0	0	2		6.8800
28.9660	3.0800	2	1	0	9.4096	
32.9020	2.7200	3	0	0	9.4224	
39.8180	2.2620	3	1	0	9.4175	
44.3690	2.0400	4	0	0	9.4224	
48.6230	1.8710	3	2	0	9.4172	
51.2830	1.7800	4	1	0	9.4189	
53.1430	1.7220	0	0	4		6.8880
59.9380	1.5420	4	2	0	9.4218	
63.4430	1.4650	5	1	0	9.4186	
Average						6.8849.4185

Fig. 4a shows the XRD patterns of washed Mg HA powders (washed MHA). $Mg(OH)_2$ disappeared, and no other calcium phosphate peaks were observed. Moreover, according to Fig. 4 (b), the peak corresponding to the Mg–hydroxyl band disappeared, indicating that Mg was removed from the structure. This result is consistent with the XRD pattern of the washed MHA. However, the acidic composition can destroy the stoichiometric and enhance the nonstoichiometric apatite nanostructure, thereby resulting in changes in HA characteristics, such as the degree of crystallinity, morphology, lattice parameters, and stability of the HA structure, and ultimately influence the biological response in actual applications. Thus, in this study, MHA is referred to as the as-prepared Mg HA.

Table 2
Lattice parameters of as-prepared synthesized HA powders.

2θ	**d** (A°) (for Sto-HA)	*h*	*k*	*l*	**d** (A°) (from graph)	**a** (A°)	**c** (A°)	**Δd** (A°)
18.7850	4.7200	1	1	0	4.6671	9.33428		0.05286
21.8190	4.0700	2	0	0	4.0370	9.32310		0.03298
25.8790	3.4400	0	0	2	3.4399		6.87982	0.00009
28.9660	3.0800	2	1	0	3.0765	9.39892		0.00348
32.9020	2.7200	3	0	0	2.7218	9.42859		0.00180
39.8180	2.2620	3	1	0	2.2729	9.46296		0.01093
44.3690	2.0400	4	0	0	2.0378	9.41229		0.00218
48.6230	1.8710	3	2	0	1.8748	9.43614		0.00377
51.2830	1.7800	4	1	0	1.7815	9.42655		0.00145
53.1430	1.7220	0	0	4	1.7209		6.88376	0.00106
59.9380	1.5420	4	2	0	1.5397	9.40754		0.00233
63.4430	1.4650	5	1	0	1.4577	9.37164		
0.00731								
Average						9.41808	6.88179	0.00344

Table 3
Lattice parameters of calcined synthesized HA powders.

2θ	**d** (A°) (for Sto-HA)	*h*	*k*	*L*	**d** (A°) (from graph)	**a** (A°)	**c** (A°)	**Δd** (A°)
21.8190	4.0700	2	0	0	4.0773	9.4161		0.0073
25.8790	3.4400	0	0	2	3.4425		6.8850	0.0025
28.9660	3.0800	2	1	0	3.0765	9.3989		0.0035
32.9020	2.7200	3	0	0	2.7186	9.4175		0.0014
39.8180	2.2620	3	1	0	2.2620	9.4173		
0.0000								
Average						9.4179	6.8850	0.0019

Table 4
Lattice parameters of as-prepared synthesized MHA powders.

2θ	**d** (A°) (for Sto-HA)	*h*	*k*	*l*	**d** (A°) (from graph)	**a** (A°)	**c** (A°)	**Δd** (A°)
18.7850	4.7200	1	1	0	4.7413	9.4827		0.0213
21.8190	4.0700	2	0	0	4.0810	9.4247		0.0110
25.8790	3.4400	0	0	2	3.4347		6.8694	0.0053
28.9660	3.0800	2	1	0	4.0869	9.4308		0.0069
32.9020	2.7200	3	0	0	2.7266	9.4454		0.0066
39.8180	2.2620	3	1	0	2.2707	9.4538		0.0087
44.3690	2.0400	4	0	0	2.0457	9.4486		0.0057
48.6230	1.8710	3	2	0	1.8733	9.4288		0.0023
51.2830	1.7800	4	1	0	1.7731	9.3822		0.0069
53.1430	1.7220	0	0	4	1.7134		6.8535	0.0086
59.9380	1.5420	4	2	0	1.5411	9.4161		0.0009
63.4430	1.4650	5	1	0	1.4557	9.3585		
0.0093								
Average						9.4272	6.8614	0.0061

Fig. 5a shows the XRD patterns of the MHA powders after heat treatment. The calcined powders showed a decrease in the peak width and more intense peaks with a slightly right shift in peak position compared with the as-prepared sample related to the Mg substitution. Moreover, the MgO peak is related to the calcination of the $Mg(OH)_2$ phase. The carbonate peak disappeared and the hydroxyl group peak was clearly identified, indicating the removal of Mg (Figs. 3b and 5b).

Some of the substituted Mg^{+2} were possibly integrated into the apatite lattice, whereas some were adsorbed on the surface of apatite crystals or present in other secondary phases. For some ions, only a small amount was incorporated in the apatite lattice, and the substitutions were limited [33]. The position of Mg in the HA lattice is not clearly known. Mg can occupy one of the two crystallographic calcium sites or both, referred to as Ca(I) and Ca(II), which present different local environments.

Table 5
Lattice parameters of calcined synthesized MHA powders.

2θ	d (A°) (for Sto-HA)	h	k	l	d (A°) (from graph)	a (A°)	c (A°)	Δd (A°)
18.7850	4.7200	1	1	0	4.7064	9.4128		0.0136
21.8190	2.0700	2	0	0	4.0773	9.4161		0.0073
25.8790	3.4400	0	0	2	3.4425		6.8850	0.0025
28.9660	3.0800	2	1	0	3.0849	9.4244		0.0048
32.9020	2.7200	3	0	0	2.7186	9.4175		0.0014
39.8180	2.2620	3	1	0	2.2620	9.4173		0.0000
44.3690	2.0400	4	0	0	2.0396	9.4203		0.0004
48.6230	1.8710	3	2	0	1.8719	9.4215		0.0009
51.2830	1.7800	4	1	0	1.7808	9.4231		0.0008
53.1430	1.7220	0	0	4	1.7209		6.8838	0.0011
59.9380	1.5420	4	2	0	1.5425	9.4247		0.0005
63.4430	1.4650	5	1	0	1.4722	9.4647		
0.0072								
Average						9.4242	6.8844	0.0020

Table 6
Lattice parameters of synthesized samples and standard HA (JCPDS 09-0432).

Samples	a (A°)	c (A°)	Δd (A°)
Standard HA(JCPDS no. 09-0432)9.41856.8840.0000			
HA	9.4181	6.8818	0.0034
MHA	9.4272	6.8614	0.0061
Calcined HA	9.417	6.885	0.0019
Calcined MHA	9.4242	6.8844	0.0020

Table 7
The degree of crystallinity of synthesized powders.

Type of powder	$2\theta^\circ$	**Variable**	**Intensity (counts)**	**Crystallinity**	
	32.88	I_{300}	31.993	X_c	%
HA				0.4688	46.88
	32.56	$V_{112/300}$	16.996		
Calcined HA	32.92	I_{300}	136.97	0.9781	97.81
	32.6	$V_{112/300}$	2.9993		
MHA	32.82	I_{300}	48.989	0.3878	38.78
	32.66	$V_{112/300}$	29.993		
Calcined MHA	32.92	I_{300}	128.97	0.969	96.9
	32.62	$V_{112/300}$	3.9991		

Table 8
Crystallite size of synthesized powders.

Sample	**Crystallite size (nm)**			
	00 2	**31 0**	**22 2**	**Average**
HA	40.756	46.911	48.065	45.244
Calcined HA	37.05	60.352	–	48.701
MHA	23.976	52.785	39.355	38.706
Calciend MHA	40.755	35.205	39.335	38.432

Some authors have proposed that Mg enters the Ca(II) site, whereas others in the Ca(I) site [18].

The lattice parameters of all samples are shown in Tables 1–5. Moreover, as shown in Table 6, the averages of calculated parameters were compared to the lattice parameters of standard HA (JCPDS no. 09-0432). The XRD and FTIR analyses of washed Mg HA showed that the powders contained apatitic structure without any calcium phosphate secondary phase; thus, these changes in apatite lattice parameters and structure is related to Mg incorporation into the apatite structure.

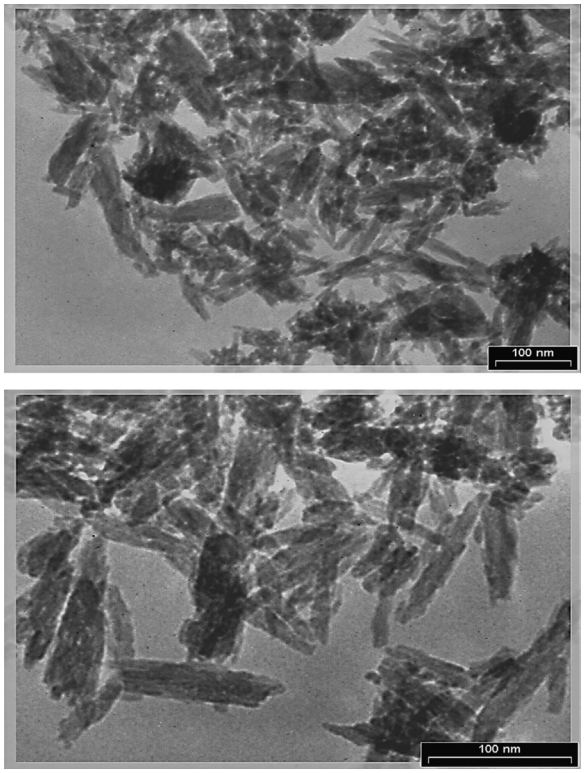

Fig. 6. TEM images of samples: (a) HA and (b) MHA.

According to Table 6, substitution of Mg can reduce the c lattice constant of stoichiometric HA (0.33%) [34,35]. Consequently, the effect of Mg substitution on the c lattice parameters is about three times greater than its effect on a lattice constant. In terms of biological issues, the change of c constant is more effective because HA is grown primarily in the c direction [36].

Therefore, Mg is expected to have a significant effect on HA growth. Table 8 indicates an increase in *d*-spacings of purified Mg-substituted HA. Mg is expected to be slightly smaller than Ca, which may result in stresses and changing *d*-spacing in the HA structure.

The *a* lattice constant of Mg-substituted apatite increased in both calcined and uncalcined samples; while in the as-prepared HA the *a* lattice constant is almost the same as that of stoichiometric HA. Hence, substitution of Mg resulted in small change (~0.1%) in apatite structure, and the value of changes in *a* constant decreased in calcined samples which is in agreement with previous studies [37].

Table 7 shows the degree of crystallinity of synthesized powders, which was increased after heat treatment. Moreover, Mg substitution reduced the degree of crystallinity of HA powders, as reported by Landi et al. [25]. This supports the fact that incorporation of Mg into the HA structure does not encourage the crystallization of hydroxyapatite.

As shown in Table 8, these results clearly indicate that the average crystallite size of HA decreased because of Mg substitution which acted as a growth inhibitor. The TEM micrographs of the HA and MHA samples are illustrated in Fig. 6. The images show that both HA and MHA crystals exhibit elongated nanorod morphology with an aspect ratio approximately equal to 10:1. Although the MHA crystals seem to be a bit smaller than HA crystals, no significant difference in crystallite size of two samples was revealed. Furthermore, TEM reveals that the actual size of the precipitated crystals (30–100 nm in length and 10–20 nm in width) are different from those calculated as an average based on XRD results (Table 8). This difference could be attributed to the fact that a given particle observed by TEM could be the result of the aggregation of several small particles, which the XRD analysis does differentiate. Furthermore, feature size in microstructure strongly depends on several factors such as kinematic and dynamic conditions, and could be different from the actual size due a number of reasons.

SEM images of samples are shown in Fig. 7. Numerous agglomerations of small spherical particles in nanometric scale between 70 nm and 130 nm were observed, which were larger than those approximated by the Scherrer equation (Table 8).

This difference in particle size is consistent with carbonate substitution in the HA structure. Moreover, planes containing the carbonate groups would be closer to Mg cations (smaller) than to Ca cations (larger) [38]. Thus, particle size in Mg carbonate HA was smaller than carbonate HA particle size, suggesting that to some extent Mg inhibits grain growth in HA.

Fig. 8 shows the SEM–EDX results of MHA sample. The EDX results clearly show the presence of Mg and C, as well as calcium, phosphorous, and oxygen in the structure. These results were consistent with XRD and FTIR results.

The line-scan EDX analysis of MHA is shown in Fig. 9. The even distribution of magnesium and carbonate ions can be seen clearly. Fig. 10 shows the elemental distribution maps (dot maps) of Mg-substituted HA powders. Uniform distribution of Mg and C as trace elements in the HA structure were observed, which is consistent with the line-scan EDX results.

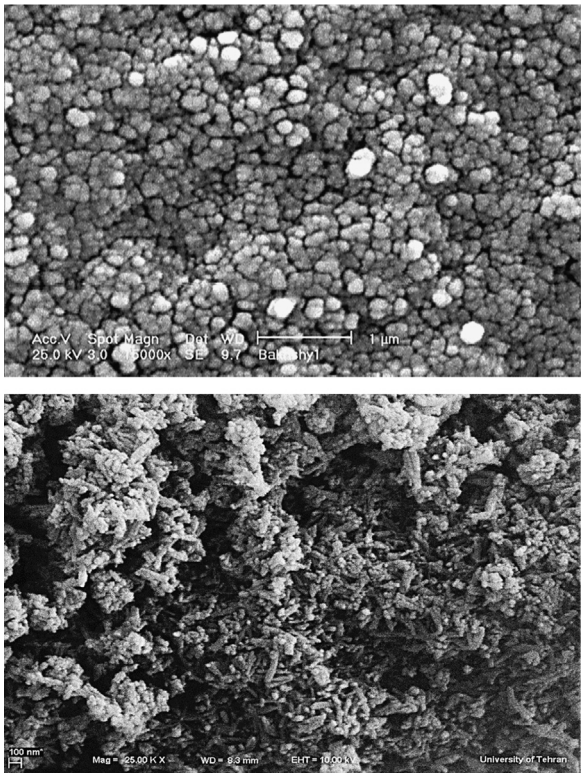

Fig. 7. SEM micrographs of samples: (a) HA and (b) MHA.

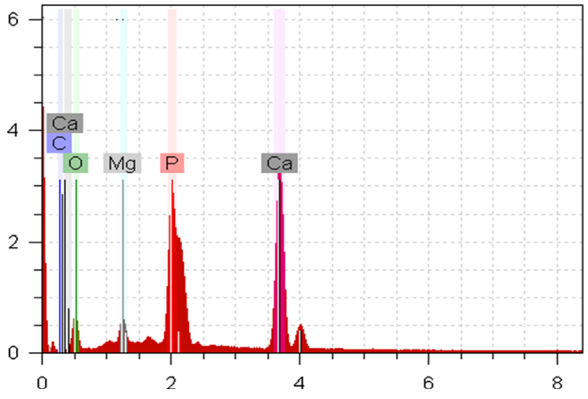

Fig. 8. SEM–EDX result of MHA powders.

4. Conclusion

Stoichiometric HA powders were prepared by wet chemical method at room temperature. Magnesium ions were successfully incorporated in the HA structure. Mg was uniformly distributed in the HA lattice between Ca sites in bulk and surface of HA crystals. The effect of Mg incorporation on HA structure was studied on lattice constants, the degree of crystallinity, and the crystal size. Mg substitution decreased the *c* lattice parameter and slightly increased the *a* lattice parameter. In addition, the degree of crystallinity and the size of crystals of the doped HA samples decreased due to the incorporation of Mg ions into the host lattice. The presence of impurity ions in the HA host lattice did not alter the high-temperature phase stability of hydroxyapatite that is often a

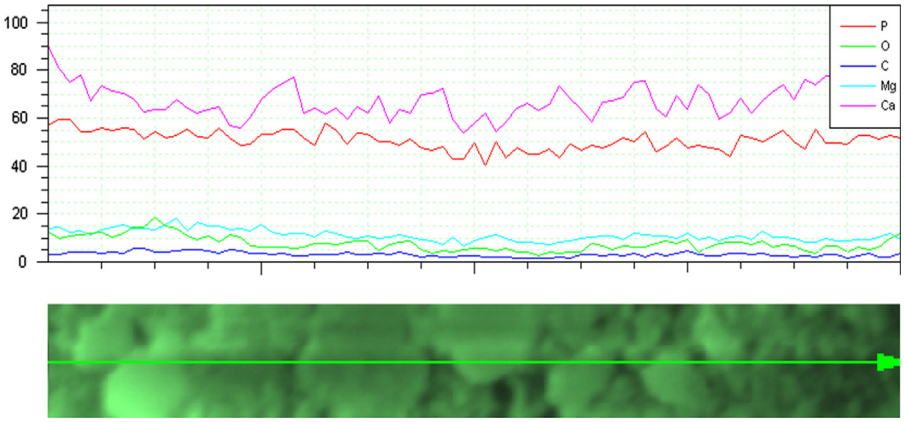

Fig. 9. Line-scan EDX result of MHA powders over a 10 μm length of samples.

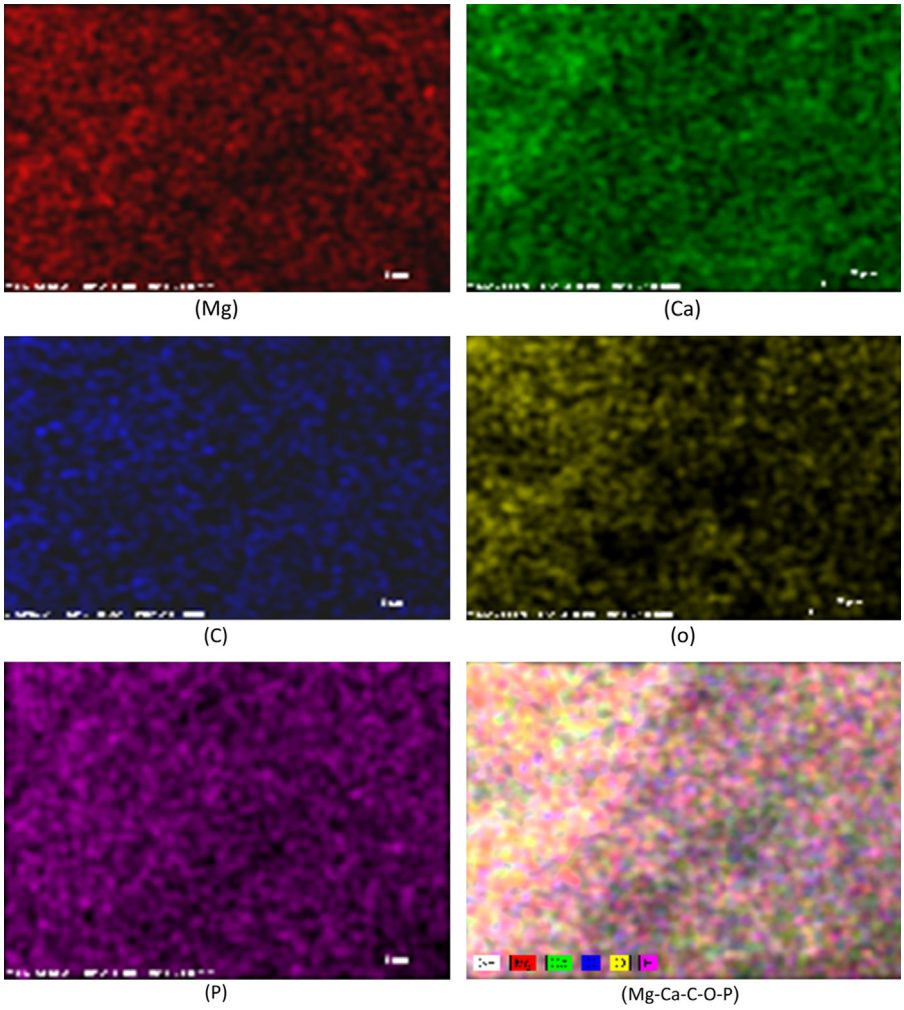

Fig. 10. Elemental distribution maps (dot maps) of MHA powder.

requirement for ceramic processing. In both HA and MHA samples, the calcium phosphate phase remained as a single-phase hexagonal calcium hydroxyapatite before and after heat treatment.

Acknowledgment

This study was supported by High Impact Research UM/MOHE/HIR Project no. D000010-16001.

References

[1] A. Farzadi, M. Solati-Hashjin, F. Bakhshi, A. Aminian, Synthesis and characterization of hydroxyapatite/β-tricalcium phosphate nanocomposites using microwave irradiation, Ceram. Int. 37 (1) (2011) 65–71.

[2] D. Bellucci, A. Sola, M. Gazzarri, F. Chiellini, V. Cannillo, A new hydroxyapatite-based biocomposite for bone replacement, Mater. Sci. Eng.: C 33 (3) (2013) 1091–1101.

[3] H. Wang, W. Zhi, X. Lu, X. Li, K. Duan, R. Duan, Y. Mu, J. Weng, Comparative studies on ectopic bone formation in porous hydroxyapatite scaffolds with complementary pore structures, Acta Biomater. 9 (9) (2013) 8413–8421 ⟨http://dx.doi.org/10.1016/j.actbio.2013.05.026⟩.

[4] B. Nasiri-Tabrizi, A. Fahami, R. Ebrahimi-Kahrizsangi, A comparative study of hydroxyapatite nanostructures produced under different milling conditions and thermal treatment of bovine bone, J. Ind. Eng. Chem. 20 (1) (2014) 246–258 ⟨http://dx.doi.org/10.1016/j.jiec.2013.03.041⟩.

[5] M. Sadat-Shojai, M.-T. Khorasani, E. Dinpanah-Khoshdargi, A. Jamshidi, Synthesis methods for nanosized hydroxyapatite with diverse structures, Acta Biomater. 9 (8) (2013) 7591–7621.

[6] A. Aminian, M. Solati-Hashjin, A. Samadikuchaksaraei, F. Bakhshi, F. Gorjipour, A. Farzadi, F. Moztarzadeh, M. Schmücker, Synthesis of silicon-substituted hydroxyapatite by a hydrothermal method with two different phosphorous sources, Ceram. Int. 37 (4) (2011) 1219–1229.

[7] J. Kolmas, A. Jaklewicz, A. Zima, M. Bućko, Z. Paszkiewicz, J. Lis, A. Ślósarczyk, W. Kolodziejski, Incorporation of carbonate and magnesium ions into synthetic hydroxyapatite: the effect on physicochemical properties, J. Mol. Struct. 987 (1–3) (2011) 40–50.

[8] H. Eslami, M. Solati-Hashjin, M. Tahriri, The comparison of powder characteristics and physicochemical, mechanical and biological properties between nanostructure ceramics of hydroxyapatite and fluoridated hydroxyapatite, Mater. Sci. Eng.: C 29 (4) (2009) 1387–1398.

[9] X. Lijuan, J. Liuyun, J. Lixin, X. Chengdong, Synthesis of Mg-substituted hydroxyapatite nanopowders: effect of two different magnesium sources, Mater. Lett. 106 (0) (2013) 246–249.

[10] Y. Cai, S. Zhang, X. Zeng, M. Qian, D. Sun, W. Weng, Interfacial study of magnesium-containing fluoridated hydroxyapatite coatings, Thin Solid Films 519 (15) (2011) 4629–4633.

[11] P.R. Larson, A.S. Madden, A.C. Tas, Non-stirred synthesis of Na- and Mg-doped, carbonated apatitic calcium phosphate, Ceram. Int. 39 (2) (2013) 1485–1493.

[12] T.-W. Kim, H.-S. Lee, D.-H. Kim, H.-H. Jin, K.-H. Hwang, J.K. Lee, H.-C. Park, S.-Y. Yoon, In situ synthesis of magnesium-substituted biphasic calcium phosphate and in vitro biodegradation, Mater. Res. Bull. 47 (9) (2012) 2506–2512.

[13] A. Gozalian, A. Behnamghader, M. Daliri, A. Moshkforoush, Synthesis and thermal behavior of Mg-doped calcium phosphate nanopowders via the sol gel method, Sci. Iran. 18 (6) (2011) 1614–1622.

[14] S. Kannan, J. Ferreira, Synthesis and thermal stability of hydroxyapatite-β-tricalcium phosphate composites with cosubstituted sodium, magnesium, and fluorine, Chem. Mater. 18 (1) (2006) 198–203.

[15] E. Landi, A. Tampieri, M. Mattioli-Belmonte, G. Celotti, M. Sandri, A. Gigante, P. Fava, G. Biagini, Biomimetic Mg- and Mg, CO_3^{2-} substituted hydroxyapatites: synthesis characterization and in vitro behaviour, J. Eur. Ceram. Soc. 26 (13) (2006) 2593–2601.

[16] M. Kheradmandfard, M.H. Fathi, M. Ahangarian, E. Mohammadi Zahrani, In vitro bioactivity evaluation of magnesium-substituted fluorapatite nanopowders, Ceram. Int. 38 (1) (2012) 169–175.

[17] M.-J. Jiao, X.-X. Wang, Electrolytic deposition of magnesium-substituted hydroxyapatite crystals on titanium substrate, Mater. Lett. 63 (27) (2009) 2286–2289.

[18] D. Laurencin, N. Almora-Barrios, N.H. de Leeuw, C. Gervais, C. Bonhomme, F. Mauri, W. Chrzanowski, J.C. Knowles, R.J. Newport, A. Wong, Z. Gan, M.E. Smith, Magnesium incorporation into hydroxyapatite, Biomaterials 32 (7) (2011) 1826–1837.

[19] I. Cacciotti, A. Bianco, M. Lombardi, L. Montanaro, Mg-substituted hydroxyapatite nanopowders: synthesis, thermal stability and sintering behaviour, J. Eur. Ceram. Soc. 29 (14) (2009) 2969–2978.

[20] A.M. Pietak, J.W. Reid, M.J. Stott, M. Sayer, Silicon substitution in the calcium phosphate bioceramics, Biomaterials 28 (28) (2007) 4023–4032.

[21] E. Landi, G. Logroscino, L. Proietti, A. Tampieri, M. Sandri, S. Sprio, Biomimetic Mg-substituted hydroxyapatite: from synthesis to in vivo behaviour, J. Mater. Sci.: Mater. Med. 19 (1) (2008) 239–247.

[22] L. Bertinetti, A. Tampieri, E. Landi, G. Martra, S. Coluccia, Punctual investigation of surface sites of HA and magnesium-HA, J. Eur. Ceram. Soc. 26 (6) (2006) 987–991.

[23] F. Ren, Y. Leng, R. Xin, X. Ge, Synthesis, characterization and ab initio simulation of magnesium-substituted hydroxyapatite, Acta Biomater. 6 (7) (2010) 2787–2796.

[24] H. Eslami, M. Tahriri, F. Bakhshi, Synthesis and characterization of nanocrystalline hydroxyapatite obtained by the wet chemical technique, Mater. Sci.-Pol. 28 (1) (2010).

[25] E. Landi, A. Tampieri, G. Celotti, S. Sprio, Densification behaviour and mechanisms of synthetic hydroxyapatites, J. Eur. Ceram. Soc. 20 (14–15) (2000) 2377–2387.

[26] C. Botelho, M. Lopes, I. Gibson, S. Best, J. Santos, Structural analysis of Si-substituted hydroxyapatite: zeta potential and X-ray photoelectron spectroscopy, J. Mater. Sci.: Mater. Med. 13 (12) (2002) 1123–1127.

[27] A. Riva, G. Camino, L. Fomperie, P. Amigouet, Fire retardant mechanism in intumescent ethylene vinyl acetate compositions, Polym. Degrad. Stab. 82 (2) (2003) 341–346.

[28] Y. Cai, J. Xue, D. Polya, A Fourier transform infrared spectroscopic study of Mg-rich, Mg-poor and acid leached palygorskites, Spectrochim. Acta Part A: Mol. Biomol. Spectrosc. 66 (2) (2007) 282–288.

[29] M. Foster, M. Furse, D. Passno, An FTIR study of water thin films on magnesium oxide, Surf. Sci. 502 (2002) 102–108.

[30] J.-P. Hsu, A. Nacu, Preparation of submicron-sized $Mg(OH)_2$ particles through precipitation, Colloids Surf. A: Physicochem. Eng. Aspects 262 (1) (2005) 220–231.

[31] Z. Wang, G. Wu, Y. Hu, Y. Ding, K. Hu, W. Fan, Thermal degradation of magnesium hydroxide and red phosphorus flame retarded polyethylene composites, Polym. Degrad. Stab. 77 (3) (2002) 427–434.

[32] W.L. Suchanek, K. Byrappa, P. Shuk, R.E. Riman, V.F. Janas, K. S. TenHuisen, Preparation of magnesium-substituted hydroxyapatite powders by the mechanochemical–hydrothermal method, Biomaterials 25 (19) (2004) 4647–4657.

[33] A. Bigi, G. Falini, E. Foresti, A. Ripamonti, M. Gazzano, N. Roveri, Magnesium influence on hydroxyapatite crystallization, J. Inorg. Biochem. 49 (1) (1993) 69–78.

[34] E. Bertoni, A. Bigi, G. Cojazzi, M. Gandolfi, S. Panzavolta, N. Roveri, Nanocrystals of magnesium and fluoride substituted hydroxyapatite, J. Inorg. Biochem. 72 (1) (1998) 29–35.

[35] S. Kannan, I. Lemos, J. Rocha, J. Ferreira, Synthesis and characterization of magnesium substituted biphasic mixtures of controlled hydroxyapatite/β-tricalcium phosphate ratios, J. Solid State Chem. 178 (10) (2005) 3190–3196.

[36] N. Kanzaki, K. Onuma, G. Treboux, S. Tsutsumi, A. Ito, Inhibitory effect of magnesium and zinc on crystallization kinetics of hydroxyapatite (0001) face, J. Phys. Chem. B 104 (17) (2000) 4189–4194.

[37] I. Gibson, W. Bonfield, Preparation and characterization of magnesium/carbonate co-substituted hydroxyapatites, J. Mater. Sci.: Mater. Med. 13 (7) (2002) 685–693.

[38] J. Deelman, Low-Temperature Formation of Dolomite and Magnesite, Compact Disc Publications, Eindhoven, The Netherlands, 2003.